LETTER

doi:10.1038/nature12607

Coherent Raman spectro-imaging with laser frequency combs

Takuro Ideguchi[1]*, Simon Holzner[1]*, Birgitta Bernhardt[1,3], Guy Guelachvili[2], Nathalie Picqué[1,2,3] & Theodor W. Hänsch[1,3]

Advances in optical spectroscopy and microscopy have had a profound impact throughout the physical, chemical and biological sciences. One example is coherent Raman spectroscopy, a versatile technique interrogating vibrational transitions in molecules. It offers high spatial resolution and three-dimensional sectioning capabilities that make it a label-free tool[1,2] for the non-destructive and chemically selective probing of complex systems. Indeed, single-colour Raman bands have been imaged in biological tissue at video rates[3,4] by using ultra-short-pulse lasers. However, identifying multiple, and possibly unknown, molecules requires broad spectral bandwidth and high resolution. Moderate spectral spans combined with high-speed acquisition are now within reach using multichannel detection[5] or frequency-swept laser beams[6–9]. Laser frequency combs[10] are finding increasing use for broadband molecular linear absorption spectroscopy[11–15]. Here we show, by exploring their potential for nonlinear spectroscopy[16], that they can be harnessed for coherent anti-Stokes Raman spectroscopy and spectro-imaging. The method uses two combs and can simultaneously measure, on the microsecond timescale, all spectral elements over a wide bandwidth and with high resolution on a single photodetector. Although the overall measurement time in our proof-of-principle experiments is limited by the waiting times between successive spectral acquisitions, this limitation can be overcome with further system development. We therefore expect that our approach of using laser frequency combs will not only enable new applications for nonlinear microscopy but also benefit other nonlinear spectroscopic techniques.

Coherent anti-Stokes Raman spectroscopy (CARS) is a nonlinear four-wave mixing process, which is coherently driven when the energy difference between a pump laser and a Stokes laser is resonant with a Raman active molecular transition. Scattering off the probe beam generates the high-frequency-shifted anti-Stokes signal, which is enhanced by many orders of magnitude relative to spontaneous Raman scattering signals. In our technique of dual-comb CARS, we harness two femtosecond lasers with repetition frequencies $f + \delta f$ and f to irradiate a sample. In the time domain (Fig. 1a), a pulse from the first laser coherently excites a molecular vibration of period $1/f_{\mathrm{vib}}$ that is longer than the pulse duration and the coherently vibrating molecules give rise[17] to an oscillating refractive index modulated at the vibrational frequency (Fig. 1b). A pulse of the second laser probes the sample with a time separation Δt that increases linearly from pulse pair to pulse pair. If this second pulse (for simplicity also taken to be short compared with the molecular vibration period[18]) arrives after a full molecular period $1/f_{\mathrm{vib}}$, the vibration amplitude is increased and the back-action on the probe pulse is a spectral shift towards lower frequencies. If it arrives after half a period, the vibration amplitude is damped and the pulse experiences a shift towards higher frequencies. As long as the pulse separation Δt remains shorter than the coherence time of the molecular oscillation, an intensity modulation of frequency $f_{\mathrm{vib}}\delta f/f$ is thus observed in the transmitted probe radiation after a spectral edge filter. The two femtosecond lasers have a symmetrical function: the sign of time separation Δt between the pulses changes every $1/(2\delta f)$. A theoretical description of such a time-resolved CARS signal can be found in ref. 19.

In the frequency domain (Fig. 1c, d), the two frequency comb generators produce an optical spectrum consisting of several hundred thousand perfectly evenly spaced spectral lines. Their frequencies may be described by

$$f^{(1)}{}_m = m(f + \delta f) + f_{\mathrm{ceo}}$$

$$f^{(2)}{}_{m'} = m'f + f'_{\mathrm{ceo}}$$

where m and m' are integers, and f_{ceo} and f'_{ceo} are the carrier-envelope offset frequencies.

The frequency differences within each comb form regular combs themselves with vanishing carrier-envelope offset frequencies and line spacings of $f + \delta f$ and f, respectively. For instance, for comb 1 all pairs of lines with $m - n = k$ contribute to the same difference frequency $k(f + \delta f)$. Each of the difference frequency combs resonantly excites a molecular level of frequency f_{vib} by means of Raman-like two-photon excitation whenever a difference frequency comes close to f_{vib}; that is, when $k \approx f_{\mathrm{vib}}/f$. The excitations by the two combs interfere and modulate the molecular vibration at a beat note frequency $k\delta f = f_{\mathrm{vib}}\delta f/f$. The two-photon excitation leads to a resonant enhancement of the third-order nonlinear susceptibility observed by means of the anti-Stokes radiation. The intensity of the generated broadband anti-Stokes radiation is modulated at the beat note frequency $f_{\mathrm{vib}}\delta f/f$. When several vibrational levels ($f_{\mathrm{vib1}}, f_{\mathrm{vib2}}, \ldots$) are excited, the composite modulation contains all the beating frequencies ($f_{\mathrm{vib1}}\delta f/f$, $f_{\mathrm{vib2}}\delta f/f, \ldots$) representative of the involved levels. The Raman excitation spectrum is revealed by Fourier transformation of the intensity recorded against time. The spectrum is mapped in the radiofrequency domain by the downconversion factor $\delta f/f$ (typically of the order of 10^{-7} to 10^{-6}). This permits rapid measurement time and efficient signal processing. Absolute calibration of the Raman shifts is achieved by dividing the radiofrequencies by the downconversion factor, which is easy to measure accurately. The carrier-envelope offsets cancel and do not have to be measured or controlled. This notably simplifies the experimental implementation and the calibration procedure. Similar modulation transfer phenomena have been exploited in experiments using a single femtosecond laser and a phase-modulation pulse shaper[20] or a Michelson interferometer[21–23], but measurement times were fundamentally limited either by the sweep period of the phase modulation or by the mechanical motion in the Michelson interferometer. Our motionless frequency-comb-based technique enables more than 1,000-fold shorter acquisition times (see also Supplementary Information), and a spectral

[1]Max-Planck-Institut für Quantenoptik, Hans-Kopfermann-Strasse 1, 85748 Garching, Germany. [2]Institut des Sciences Moléculaires d'Orsay, CNRS, Bâtiment 350, Université Paris-Sud, 91405 Orsay, France. [3]Ludwig-Maximilians-Universität München, Fakultät für Physik, Schellingstrasse 4/III, 80799 München, Germany.
*These authors contributed equally to this work.

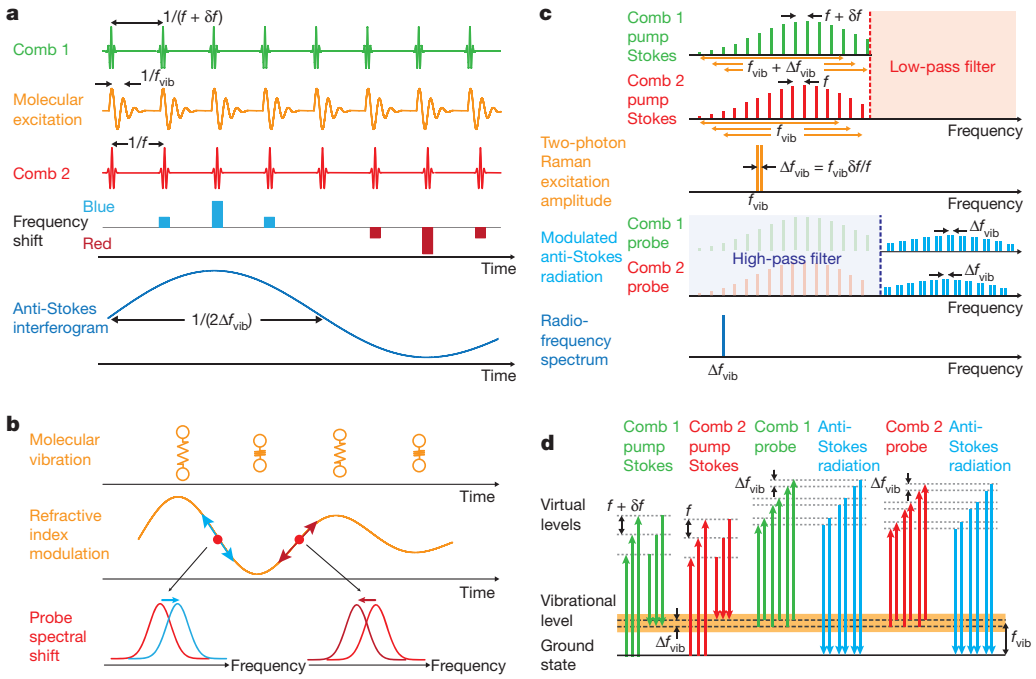

Figure 1 | Principle of dual-comb CARS. Δf_{vib} stands for $f_{vib}\delta f/f$. **a**, Time-domain representation in the limit of a molecular decoherence time that is shorter than the time interval between two laser pulses. The train of pulses of laser frequency comb 1 periodically excites the molecular vibration, which is probed by the pulses of laser frequency comb 2 with a linearly increasing time delay. The resulting filtered anti-Stokes radiation provides the interferogram. The two combs have a symmetric function. In the figure, only the situation in which the delay between the pulses of comb 2 and those of comb 1 is positive is displayed. **b**, When the probe pulse is short compared with the molecular oscillation (impulsive stimulated Raman scattering), the refractive index modulation of the sample—induced by the pump and Stokes beam—shifts the probe spectrum alternatively towards lower and higher frequencies. **c**, Frequency-domain representation in the limit of a comb line spacing that is larger than the resonant Raman excitation bandwidth. The two frequency combs modulate the excitation amplitude of the molecular vibration with a frequency Δf_{vib}. This modulation is then transferred by the combs to the anti-Stokes radiation. For simplicity, the Raman excitations are represented as narrow lines. **d**, Energy-level diagram, illustrating the four-wave mixing that leads to intensity-modulated anti-Stokes radiation.

resolution and spectral span only limited by the measurement time and the spectral bandwidth of the femtosecond lasers.

Figure 2 sketches the experimental setup (see Methods), which is similar to that used in dual-comb absorption spectroscopy[11–13] except for dispersion management and spectral filtering to isolate the CARS signal from the comb beams. As the Raman-like two-photon excitation involves virtual energy levels, dispersion decreases both the spectral span and the excitation efficiency. The time-domain interference signal—the interferogram—is periodic. Every $1/\delta f$, a strong burst mostly contains the non-resonant four-wave mixing signal resulting from the interference between the overlapping pulses of the two combs. A reproducible modulation (Fig. 3a), due to the CARS signal only, follows the burst and has a duration proportional to the coherence time of the sample transitions. A time-windowed portion of the interferogram, which excludes the interferometric non-resonant contribution, is Fourier transformed. The width of the window is chosen according to the desired spectral resolution (see Methods for a detailed explanation of the recording parameters). The resulting spectra (Fig. 3b–d) span Raman shifts from 200 cm^{-1} to 1,400 cm^{-1}. The non-resonant background, which strongly lowers the sensitivity of CARS, is entirely suppressed, as in other specific CARS schemes[20–23].

We illustrate acquisition times with three spectra at an apodized resolution of 4 cm^{-1} and recorded with $\delta f = 100$ Hz (Fig. 3b) or 5 Hz (Fig. 3c, d) for a mixture of hexafluorobenzene, nitrobenzene, nitromethane and toluene in a cuvette 5 mm long. The spectra involve no averaging and were measured in 14.8 μs (Fig. 3b) and 295.5 μs (Fig. 3c, d); the number of individual spectral elements (defined as the spectral span divided by the resolution) for all three spectra is 300. The signal-to-noise ratio culminates at 1,000 for the most intense blended line of toluene and nitrobenzene in Fig. 3c. Recorded under different experimental conditions, the three spectra show great similarities in line position and relative intensity.

Imaging capabilities are illustrated with a capillary plate (25-μm diameter holes, thickness 500 μm) filled with a mixture of hexafluorobenzene, nitromethane and toluene. For each pixel, we measure an interferogram within 12 μs to obtain a spectrum at an apodized resolution of

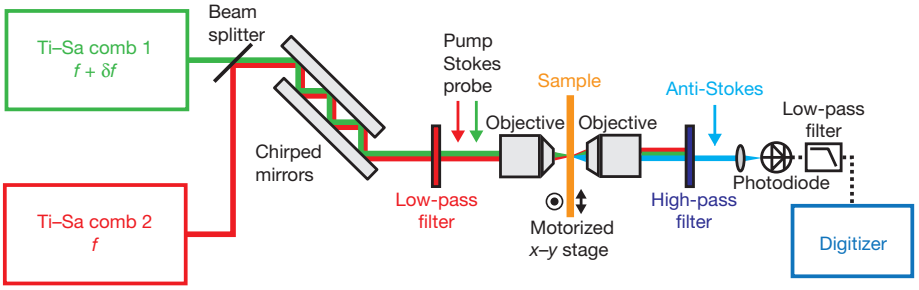

Figure 2 | Experimental setup for dual-comb CARS spectro-imaging. See Methods for details. The colour code is consistent with that of Fig. 1. Ti–Sa, titanium–sapphire.

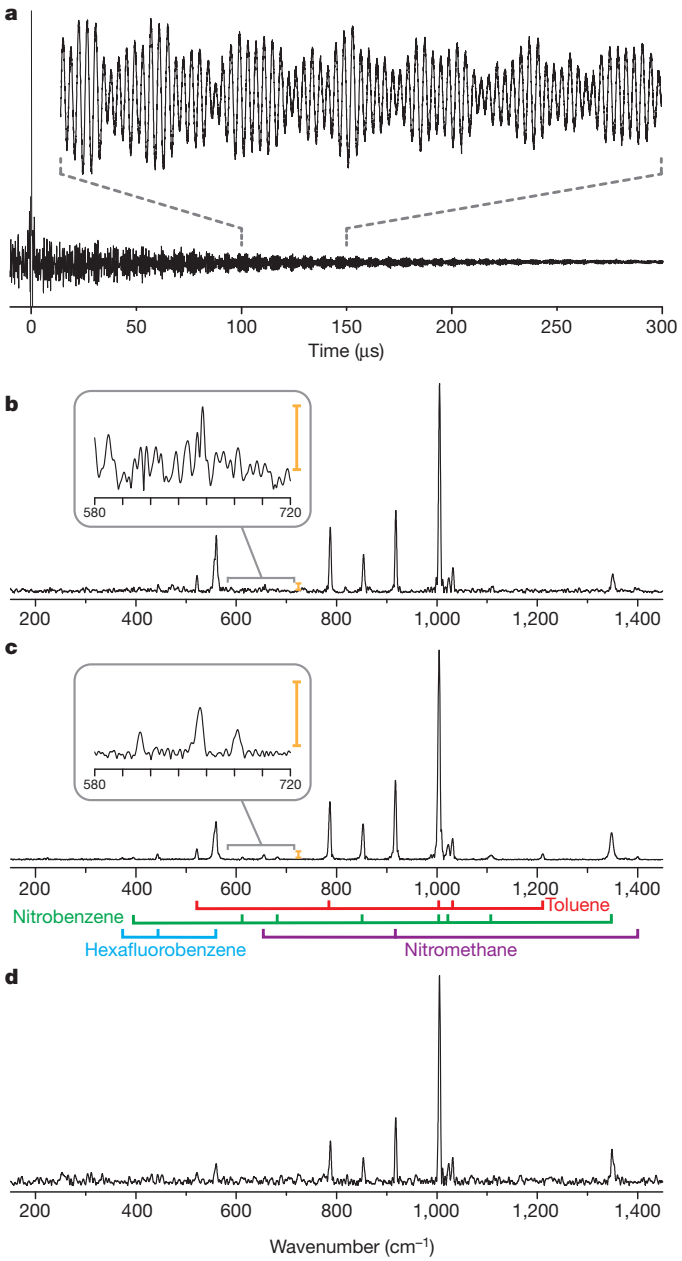

Figure 3 | High-resolution dual-comb CARS of a mixture of liquid chemicals. **a**, Unaveraged interferogram showing the non-resonant interference signal around the zero time delay and the interferometric modulation of the vibrational transitions shown in **c** ($\delta f = 5$ Hz; energy per pulse 3 nJ). **b**, Dual-comb CARS unaveraged spectrum ($\delta f = 100$ Hz; measurement time 14.8 μs; apodized resolution 4 cm^{-1}; energy per pulse 3 nJ). **c**, Dual-comb CARS unaveraged spectrum ($\delta f = 5$ Hz; measurement time 295.5 μs; apodized resolution 4 cm^{-1}; energy per pulse 3 nJ). **d**, Dual-comb CARS unaveraged spectrum ($\delta f = 5$ Hz; measurement time 295.5 μs; apodized resolution 4 cm^{-1}; energy per pulse 0.5 nJ). The insets in **b** and **c** magnify the vertical scale tenfold.

10 cm^{-1}. The total measurement time of 40.5 s for the 45×45 μm^2 hyperspectral image corresponds to an acquisition rate of 50 pixels s^{-1}; it is limited by the refresh rate of the interferograms, although the entire sampling time of the interferograms—which are Fourier transformed to give the spectral hypercube in Fig. 4—lasts only 24.3 ms.

Taken together, the above proof-of-principle experiments demonstrate the potential of our method for the rapid acquisition of both high-resolution spectra spanning a broad bandwidth and hyperspectral images of vibrational transitions. A unique feature of our technique is its multiplex nature: all the spectral elements are measured at

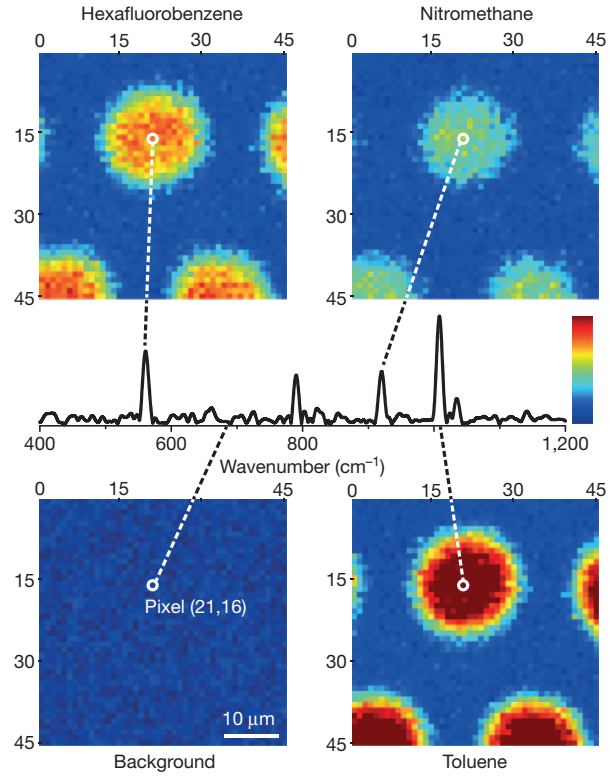

Figure 4 | Hyperspectral image of a capillary plate with holes filled with a chemical mixture. Each of the 2,025 pixels of the hyperspectral cube corresponds to a spectrum at 10 cm^{-1} apodized resolution measured within 12 μs at a fixed spatial location and provides the spectral signature of compounds present in this part of the sample. Scale numbers on the images indicate pixels; the spectrum shown in the centre corresponds to pixel (21,16). Each spectral element of the cube may be plotted as an image (that is, intensity for all pixels at a fixed wavenumber) similar to the four that are shown and provides the spatial quantitative distribution of a given compound with a distinguishable spectral signature at that wavenumber.

the same time on a single photodetector, which ensures consistency of the spectra. Moreover, the frequency combs guarantee the reproducibility and accuracy of the wavenumber scale. However, a major limitation in the present proof-of-principle experiments is the low duty cycle (the ratio between the time it takes to measure an interferogram and the time before the next interferogram is measured), which for the spectro-imaging experiments shown in Fig. 4 is only 6×10^{-4}. The interferogram refresh time is the inverse of the difference of the laser repetition frequencies $1/\delta f$, whereas the spectral information is only collected when the delay between the pairs of pulses is shorter than the coherent molecular ringing time (see Supplementary Information for more detailed discussion). One solution would be to use combs with a larger line spacing, which could allow the duty cycle of interferogram acquisition to approach unity while keeping measurement times and signal-to-noise ratios similar to those in Figs 3 and 4. Frequency comb generators based on solid-state lasers with a short cavity[24] or on chip-scale microresonators[25] might offer a route towards realizing such high duty cycle experiments. For microscopy experiments, scanning the laser beam with a galvanometric mirror rather than the sample stage provides a straightforward way to speed up the mapping process. High-speed cameras (more than 10^6 frames s^{-1}) could even allow real-time hyperspectral dual-comb CARS imaging. There is also scope for improvements that would affect the signal itself. For example, a more sophisticated dispersion management, particularly of third-order dispersion, would enhance the signal-to-noise ratio. This could be complemented with fast synchronous or differential detection schemes that might further decrease the noise level. Finally, few-cycle oscillators or spectral broadening with nonlinear fibres will expand the spectral span of the setup.

Several schemes exploiting coherent Raman scattering for novel spectroscopy and microscopy applications have recently emerged, and we expect that their combination with our method will deliver techniques with improved performance and utility. For example, our dual-comb approach could benefit surface-enhanced[26,27] CARS measurements or studies of Raman optical activity[28]. Moreover, exciting imaging capabilities might arise when extending our method to exploit either near-field effects (for example at a metal tip[29]) or far-field effects (for example state depletion[30]) to achieve sub-wavelength spatial resolution.

METHODS SUMMARY

Two titanium–sapphire lasers (Synergy20 UHP; Femtolasers) emit 20-fs pulses centred at 12,580 cm^{-1} with energies up to 13 nJ. Both have adjustable repetition frequencies of about 100 MHz. The beams of the two lasers (Fig. 2) are combined on a beamsplitter, and a chirped mirror compressor (Layertec) compensates for the second-order dispersion induced by the optical components of the setup. Spectral filtering is applied to improve the signal-to-background ratio. A low-frequency-pass filter (ET750LP, cutoff 13,330 cm^{-1}; Chroma Technology) before the sample and a high-frequency-pass filter (3RD740SP, cutoff 13,510 cm^{-1}; Omega Optical Inc.) after the sample isolate the CARS signal that is generated by the sample after proper focusing with a lens or a microscope objective. The spectral span is thus limited on the low-energy side by the optical filters and on the high-energy side by the spectral bandwidth of the femtosecond lasers. The anti-Stokes radiation is forward-collected and focused on a silicon photodiode with a frequency bandwidth of the order of 100 MHz. The electric signal is low-pass filtered to 50 MHz to avoid aliasing. It is then amplified and digitized with a 16-bit data acquisition board (1.8×10^8 samples s^{-1}, ATS9462; Alazartech).

Online Content Any additional Methods, Extended Data display items and Source Data are available in the online version of the paper; references unique to these sections appear only in the online paper.

Received 9 February; accepted 27 August 2013.

1. Nafie, L. A. Recent advances in linear and nonlinear Raman spectroscopy. Part VI. *J. Raman Spectrosc.* **43,** 1845–1863 (2012).
2. Cheng, J. X. & Xie, X. S. (eds). *Coherent Raman Scattering Microscopy* (CRC Press, 2012).
3. Evans, C. L. *et al.* Chemical imaging of tissue *in vivo* with video-rate coherent anti-Stokes Raman scattering microscopy. *Proc. Natl Acad. Sci. USA* **102,** 16807–16812 (2005).
4. Saar, B. G. *et al.* Video-rate molecular imaging *in vivo* with stimulated Raman scattering. *Science* **330,** 1368–1370 (2010).
5. Knutsen, K. P., Messer, B. M., Onorato, R. M. & Saykally, R. J. Chirped coherent anti-Stokes Raman scattering for high spectral resolution spectroscopy and chemically selective imaging. *J. Phys. Chem. B* **110,** 5854–5864 (2006).
6. Ozeki, Y. *et al.* High-speed molecular spectral imaging of tissue with stimulated Raman scattering. *Nature Photon.* **6,** 845–851 (2012).
7. Kong, L. *et al.* Multicolor stimulated Raman scattering microscopy with a rapidly tunable optical parametric oscillator. *Opt. Lett.* **38,** 145–147 (2013).
8. Pegoraro, A. F. *et al.* Optimally chirped multimodal CARS microscopy based on a single Ti:sapphire oscillator. *Opt. Express* **17,** 2985–2996 (2009).
9. Fu, D., Holtom, G., Freudiger, C., Zhang, X. & Xie, X. S. Hyperspectral imaging with stimulated Raman scattering by chirped femtosecond lasers. *J. Phys. Chem. B* **117,** 4634–4640 (2013).
10. Hänsch, T. W. Nobel Lecture. Passion for precision. *Rev. Mod. Phys.* **78,** 1297–1309 (2006).
11. Schliesser, A., Picqué, N. & Hänsch, T. W. Mid-infrared frequency combs. *Nature Photon.* **6,** 440–449 (2012).
12. Bernhardt, B. *et al.* Cavity-enhanced dual-comb spectroscopy. *Nature Photon.* **4,** 55–57 (2010).
13. Coddington, I., Swann, W. C. & Newbury, N. R. Coherent multiheterodyne spectroscopy using stabilized optical frequency combs. *Phys. Rev. Lett.* **100,** 013902 (2008).
14. Diddams, S. A., Hollberg, L. & Mbele, V. Molecular fingerprinting with the resolved modes of a femtosecond laser frequency comb. *Nature* **445,** 627–630 (2007).
15. Thorpe, M. J. *et al.* Broadband cavity ringdown spectroscopy for sensitive and rapid molecular detection. *Science* **311,** 1595–1599 (2006).
16. Ideguchi, T., Bernhardt, B., Guelachvili, G., Hänsch, T. W. & Picqué, N. Raman-induced Kerr effect dual-comb spectroscopy. *Opt. Lett.* **37,** 4498–4500 (2012).
17. Boyd, R. W. *Nonlinear Optics* 3rd edn, Ch. 10.3 (Academic, 2008).
18. Yan, Y., Gamble, E. B. & Nelson, K. A. Impulsive stimulated scattering: general importance in femtosecond laser pulse interaction with matter, and spectroscopy applications. *J. Chem. Phys.* **83,** 5391–5399 (1985).
19. Mukamel, S. *Principles of Nonlinear Optical Spectroscopy* (Oxford Univ. Press, 1995).
20. Dudovich, N., Oron, D. & Silberberg, Y. Single-pulse coherently controlled nonlinear Raman spectroscopy and microscopy. *Nature* **418,** 512–514 (2002).
21. Weiner, A. M., Leaird, D. E., Wiederrecht, G. P. & Nelson, K. A. Femtosecond multiple-pulse impulsive stimulated Raman scattering spectroscopy. *J. Opt. Soc. Am. B* **8,** 1264–1275 (1991).
22. Volkmer, A., Book, L. D. & Xie, X. S. Time-resolved coherent anti-Stokes Raman scattering microscopy: imaging based on Raman free induction decay. *Appl. Phys. Lett.* **80,** 1505–1507 (2002).
23. Ogilvie, J. P., Beaurepaire, E., Alexandrou, A. & Joffre, M. Fourier-transform coherent anti-Stokes Raman scattering microscopy. *Opt. Lett.* **31,** 480–482 (2006).
24. Bartels, A., Heinecke, D. & Diddams, S. A. 10-GHz self-referenced optical frequency comb. *Science* **326,** 681 (2009).
25. Kippenberg, T. J., Holzwarth, R. & Diddams, S. A. Microresonator-based optical frequency combs. *Science* **332,** 555–559 (2011).
26. Steuwe, C., Kaminski, C. F., Baumberg, J. J. & Mahajan, S. Surface enhanced coherent anti-Stokes Raman scattering on nanostructured gold surfaces. *Nano Lett.* **11,** 5339–5343 (2011).
27. Frontiera, R. R., Henry, A. I., Gruenke, N. L. & Van Duyne, R. P. Surface-enhanced femtosecond stimulated Raman spectroscopy. *J. Phys. Chem. Lett.* **2,** 1199–1203 (2011).
28. Hiramatsu, K. *et al.* Observation of Raman optical activity by heterodyne-detected polarization-resolved coherent anti-Stokes Raman scattering. *Phys. Rev. Lett.* **109,** 083901 (2012).
29. Ichimura, T., Hayazawa, N., Hashimoto, M., Inouye, Y. & Kawata, S. Tip-enhanced coherent anti-Stokes Raman scattering for vibrational nanoimaging. *Phys. Rev. Lett.* **92,** 220801 (2004).
30. Cleff, C. *et al.* Ground-state depletion for subdiffraction-limited spatial resolution in coherent anti-Stokes Raman scattering microscopy. *Phys. Rev. A* **86,** 023825 (2012).

Supplementary Information is available in the online version of the paper.

Acknowledgements We thank P. Hommelhoff, M. Schultze and W. Schweinberger for the loan of optical components, and A. Hipke for experimental support. Research was conducted in the scope of the European Laboratory for Frequency Comb Spectroscopy. We acknowledge support from the Max Planck Foundation, the Munich Center for Advanced Photonics, Eurostars and the European Research Council (Advanced Investigator grant no. 267854).

Author Contributions T.I. and S.H. contributed equally to the experimental work. All authors contributed extensively to the work presented in this paper.

Author Information Reprints and permissions information is available at www.nature.com/reprints. The authors declare no competing financial interests. Readers are welcome to comment on the online version of the paper. Correspondence and requests for materials should be addressed to N.P. (nathalie.picque@mpq.mpg.de).

METHODS

Detailed experimental setup. Two titanium–sapphire lasers (Synergy20 UHP; Femtolasers) emit 20-fs pulses centred at 12,580 cm^{-1} with energies up to 13 nJ. Titanium–sapphire lasers are chosen because of their capabilities to generate ultrashort pulses in a spectral region where most samples have no or only weak absorption and where advanced photonics tools are available. Both oscillators have repetition frequencies of about 100 MHz, which can be adjusted by moving a cavity mirror mounted on a motorized translation stage and a piezoelectric transducer. The repetition frequencies are monitored with fast silicon photodiodes connected to frequency counters (53131A; Agilent). To prevent long-term drifts, the repetition frequency of each laser comb is stabilized against a radiofrequency clock by means of a mirror of the laser's cavity mounted on a piezoelectric transducer. This does not affect the quality of an individual spectrum but improves the reproducibility of the wavenumber scale of a sequence of spectra. The laser beams are linearly polarized. The pulse energy available for the spectroscopy experiments is adjusted for each laser beam individually with a combination of a half-wave plate and a polarizer. The beams of the two lasers are combined (Fig. 2) on a pellicle beamsplitter, and a chirped mirror compressor (Layertec) compensates for the second-order dispersion induced by the optical components of the setup. Spectral filtering is applied to improve the signal-to-background ratio. A low-frequency-pass optical filter (ET750LP, cutoff 13,330 cm^{-1}; Chroma Technology) before the sample and a high-frequency-pass optical filter (3RD740SP, cutoff 13,510 cm^{-1}; Omega Optical Inc.) after the sample isolate the CARS signal that is generated by the sample after proper focusing with a lens or a microscope objective. The spectral span is thus limited on the low-energy side by the optical filters and on the high-energy side by the spectral bandwidth of the femtosecond lasers. The anti-Stokes radiation is forward-collected and focused on a single silicon photodiode with a frequency bandwidth of the order of 100 MHz. The electric signal is low-pass filtered to 50 MHz to avoid aliasing. The non-interferometric signal, which occurs at the pulse repetition frequency, is also filtered out. This non-interferometric signal (CARS and non-resonant signal within a single laser pulse) is the main source of undesired background. The interferometric signal is then amplified with a wideband variable-gain voltage amplifier (DHPVA-100; FEMTO Messtechnik GmbH) and digitized with a 16-bit data acquisition board (1.8×10^8 samples s^{-1}, ATS9462; Alazartech). Apodization and Fourier transformation may be accomplished in real time with the use of field-programmable gate arrays or a posteriori with a basic desktop computer.

The data of Fig. 3 were recorded with orthogonal linear polarizations of the two laser beams. This decreased the interferometric non-resonant background, while the fast depolarization of the sample maintained the strength of the anti-Stokes signal. For the spectra of Fig. 3b, c, the focusing optics consisted of lenses with a focal length of 20 mm and required an amount of dispersion compensation of -600 fs^2. The pulse energy at the sample was 3 nJ. The spectrum of Fig. 3d was measured with a focusing lens with a focal length of 8 mm, a pulse energy of 0.5 nJ and an avalanche photodetector (APD Module C4777; Hamamatsu).

To record the hyperspectral images (Fig. 4), the difference in repetition frequencies of the two combs was set to 50 Hz and a microscope objective (LCPLN20XIR; Olympus) focused the beams on the sample, with a beam diameter of 1.9 μm and a Rayleigh length of 3.4 μm. The pulse energy at the sample was 3.8 nJ and a second-order dispersion of $-3{,}000$ fs^2 was compensated for. The sample was mounted on a motorized x–y platform (MLS203, Thorlabs) to raster scans across the sample in 1-μm steps.

Choice of recording parameters. In our experiments of coherent anti-Stokes Raman spectroscopy with two laser frequency combs, the vibrational levels that are excited in a Raman two-photon process have an energy f_{vib} that matches a frequency difference between pairs of lines of one comb. The vibration is modulated by the interference between the excitation by the two combs and is thus downconverted to the frequency $f_{vib}\delta f/f$.

The energy $f_{vib,max}$ (in hertz) of the higher-lying vibrational level that can be observed is about the spectral bandwidth of the combs ΔF (in hertz), roughly twice the full width at half-maximum of the laser spectrum:

$$f_{vib,max} = \Delta F$$

The difference δf in repetition frequencies between the two lasers must be adjusted to image the domain 0–ΔF into a radiofrequency free spectral range of 0–$f/2$ at most. Thus, to avoid aliasing, one has to choose $\delta f \leq f^2/(2\Delta F)$. For the faster recording times, δf should be chosen equal to $f^2/(2\Delta F)$. However, for signal-to-noise ratio improvement, it may be advantageous to set δf to a lower value, as illustrated in Fig. 3.

The Fourier transform of the interferometric signal provides a radiofrequency spectrum with a free spectral range equal to $\Delta F\delta f/f$ (and less than or equal to $f/2$). The Raman-shift scale is retrieved by dividing the measured radiofrequency scale by the downconversion factor $\delta f/f$.

The resolution $\delta\nu_{rf}$ (in hertz) in the radiofrequency domain, in a magnitude spectrum with triangular apodization, is given by the inverse of the measurement time T:

$$\delta\nu_{rf} = 1.8/T$$

The optical resolution $\delta\nu_{opt}$ (in hertz) of the Raman spectrum is retrieved by dividing the radiofrequency resolution $\delta\nu_{rf}$ by the downconversion factor $\delta f/f$:

$$\delta\nu_{opt} = 1.8f/(\delta fT)$$

The instrumental resolution is fundamentally limited by the line spacing f of the comb. For most mode-locked lasers the line spacing is within the range 50 MHz to 1 GHz. Thus this limitation is not an issue in most liquid-phase studies, because the width of the vibrational bands is generally broader than 100 GHz (3.3 cm^{-1}). It is, however, possible to improve the resolution by interleaving successively acquired spectra recorded with slightly different radiofrequency line spacings.

The difference δf in repetition frequencies between the two lasers also determines the interferogram refresh rate. Every $1/\delta f$ the pulse train of one laser scans the entire pulse period of the second laser comb to generate a single interferogram, which is afterwards time-windowed to provide the desired resolution. This refresh rate limits the speed of successive acquisitions and thus is currently the main limitation for fast hyperspectral imaging experiments. A detailed discussion in Supplementary Information elaborates on this difficulty and shows that frequency combs of a relatively large line spacing (1 GHz) hold promise to overcome it.

In our experiment we use lasers with a repetition frequency of about $f = 100$ MHz. When the difference of repetition frequencies of the two lasers is set to $\delta f = 100$ Hz, the downconversion factor $\delta f/f$ is 10^{-6}. The radiofrequency free-spectral range is 50 MHz and the optical free spectral range ΔF is 50 THz (1,668 cm^{-1}). A recording time of 15 μs leads to a radiofrequency resolution $\delta\nu_{rf}$ of 120 kHz, which converts to an optical resolution $\delta\nu_{opt}$ of 120 GHz (4 cm^{-1}). The refresh time of the interferograms is 10 ms.